Article

Study on the Dip Angle Effect of Asymmetric Deformation and Failure of the Gob-Side Coal–Rock Roadway in Gently Inclined Coal Seam

Lin Gao [1,2,3,4,*], Xinyu Zhan [1], Pandong Zhang [1], Zhijie Wen [4], Zhenqian Ma [1,3], Dezhong Kong [1,3], Xiangtao Kang [1,3] and Sen Han [1,3]

1   College of Mining, Guizhou University, Guiyang 550025, China; gs.xyzhan21@gzu.edu.cn (X.Z.); gs.pdzhang20@gzu.edu.cn (P.Z.); zqma@gzu.edu.cn (Z.M.); dzkong@gzu.edu.cn (D.K.); xiaokangedu@163.com (X.K.); shan1@gzu.edu.cn (S.H.)
2   Coal Mine Roadway Support and Disaster Prevention Engineering Research Center, Beijing 100083, China
3   National & Local Joint Laboratory of Engineering for Effective Utilization of Regional Mineral Resources from Karst Areas, Guiyang 550025, China
4   Key Laboratory of Mining Disaster Prevention and Control, Qingdao 266590, China; wenzhijie@sdust.edu.cn
*   Correspondence: lgao@gzu.edu.cn; Tel.: +86-13639078487

Abstract: In order to reveal the influence law of coal seam dip angle on the stability of the surrounding rock of the gob-side coal–rock roadway in a gently inclined coal seam (GCRGICS), the deformation characteristics of the surrounding rock under four different coal seam dip angles of this kind of roadway were studied by field investigation, theoretical analysis and numerical simulation. The results showed that, with the increase of the coal seam dip angle, the amount of the roadway roof subsidence and the deformation of the upper and lower side arc triangle coal along the coal–rock interface increased, and the maximum deformation was 479 and 950 mm, respectively, and the maximum slip deformation area gradually shifted from the upper side arc triangle coal to the lower side arc triangle coal. The asymmetric deformation characteristics of the surrounding rock became more and more obvious. The asymmetric deformation rate of the GCRGICS showed a V-shaped variation relationship with the coal seam dip angle, when the coal seam dip angle was 10°, the asymmetric deformation rate was the minimum, only 1.1%. The plastic zone of the surrounding rock expanded with the increase of the coal seam dip angle, and the new extension range was mainly located in the roof area of the roadway.

Keywords: dip angle of coal seam; coal–rock roadway; gob-side roadway; coal–rock interface; asymmetric deformation

1. Introduction

The occurrence conditions of coal seams in Guizhou Province are complex, most of them are (gently) inclined thin and medium-thick coal seams, resulting in a wide distribution of the coal–rock roadway in the mining area [1–4]. Due to the asymmetry and heterogeneity of the surrounding rock structures, this kind of roadway has low mechanical strength compared with the full-coal or full-rock roadway and often presents complex deformation and failure characteristics of the surrounding rock [5–7].

Some scholars have carried out relevant research on the deformation mechanism and control technology of the surrounding rock in the coal–rock roadway. Such as Wang et al. [8] who took near-horizontal coal–rock mining roadway as their research object and determined that the key to maintaining the stability of the surrounding rock of such a roadway was to control the shear slip misalignment deformation of the coal–rock interface. Liu [9] studied the stability of the surrounding rock structure of the coal–rock roadway based on FLAC^{3D} numerical simulation software and found that the loosening circle of the surrounding rock in the roadway side was the largest, and its average value was 1.5 times that of loosening circle of

the roof and floor. Yao et al. [10] studied the deformation and failure mechanism of a coal–rock roadway with extremely broken surrounding rock and found that, under the condition of passive support, the deformation and failure of the roadway were influenced by multiple effects of water absorption expansion, weak interlayer, joints, and so on, and the deformation and failure of the roadway were serious. Zhang et al. [11] analyzed the change law of the plastic zone of the surrounding rock of the coal–rock roadway with different buried depths and found that the plastic zone of the surrounding rock gradually increased with the increase of roadway buried depth, especially in the two sides and floor. Jin et al. [12] found that after the coal–rock mining roadway was dug out, when the support strength was not enough, the plastic zone development range of the surrounding rock in the process of stress balance was mainly concentrated in the two sidewalls and roof. Luo et al. [13] found that the coal–rock roadways have obvious discontinuities in the levels of the surrounding rock structure, mechanical properties, and surrounding rock deformation and rupture. Wang et al. [14] aimed at the serious deformation problem of a coal–rock roadway in China's Meihuajing coal mine and analyzed the characteristics of discontinuous surrounding rock structure and asymmetric deformation of the surrounding rock by means of geological investigation, mechanical experiment and numerical simulation. Sun et al. [15] concluded that the lack of floor control in roadway support, the weakening of rock mass strength by geological tectonic action and the water swelling of the argillaceous floor were the three main factors leading to floor heave in a coal–rock soft floor roadway. Yu et al. [16] found that, when the specimen of the coal–rock combination was under pressure, the coal body was mainly destroyed by bulging under pressure. There was a certain relative sliding trend between the coal body and the rock mass in the coal–rock roadway, and the roadway section would have uneven deformation, resulting in a large deformation or destruction of key parts. Xu. [17] studied the cross-section shape of the coal–rock roadway by numerical simulation and pointed out that the arc angle shape was better than the acute angle heterotype. Gao et al. [18] used a numerical simulation method to study the influence of different basic roof fracture forms on the stability of surrounding rock of the coal–rock roadway along the goaf in an inclined coal seam and found that the position of the basic roof fracture line on the goaf side had the least influence on the stability of the surrounding rock. Zhang et al. [19] found that the surrounding rock of the roadway arranged in thin-bedded coal–rock crossovers showed asymmetric deformation characteristics, and the deformation of floor, shoulder angle, and arch angle were severe. The conventional open and symmetrical support structures could not control the deformation of the roadway. In view of the deformation and failure characteristics of the surrounding rock of the coal–rock roadway under specific conditions, some scholars [20–24] have conducted optimization analysis and research on the support scheme and specific support parameters of the coal–rock roadway based on numerical simulation, theoretical analysis and field test.

The above research has provided useful references for the control of the surrounding rock of the near-horizontal coal–rock roadway. However, research on the mechanical mechanism and control technology of the deformation and failure of the surrounding rock of the GCRGICS in Guizhou Province has been rare. In addition, the research on the deformation mechanism of the coal–rock roadway in the existing results mostly focused on the difference in strength between the coal and the rock body in the roadway side, ignoring the influence of the dip angle on the stability of the surrounding rock. Therefore, the authors took the 1511 return air roadway of a mine in Guizhou as the research object and studied the asymmetric deformation and failure characteristics of the gob-side coal–rock roadway under different coal seam dip angles by numerical simulation, and the internal relationship between the coal seam dip angle and asymmetric deformation and the failure of the gob-side coal–rock roadway was further revealed.

2. Asymmetric Deformation Characteristics of Surrounding Rock in the Gob-Side Coal–Rock Roadway

Based on the field engineering investigation, the surrounding rock deformation of the 1511 return air roadway (GCRGICS) mainly presented the following characteristics:

(1) Continuous floor heave. Due to the infiltration of fissure water in the surrounding rock and the influx of water from the neighboring mining, the floor was seriously flooded after roof watering, and floor heave deformation was continuously produced, as shown in Figure 1a.

(2) Coal–rock interface slip dislocation. The coal–rock body at the coal–rock interface on the side of the roadway, especially at the side of the narrow coal pillar, produced an obvious slip dislocation deformation along the coal–rock interface. When it was serious, it presented the phenomenon of stepped bulging, as shown in Figure 1b.

(3) The two sides showed asymmetric deformation characteristics. It was found in the investigation that, under the existing support model, the deformation of the coal pillar side of the roadway was generally greater than that of the solid coal side, as shown in Figure 1c,d. According to the results of the field investigation, the sketch of asymmetric deformation characteristics of the roadway was drawn in Figure 2.

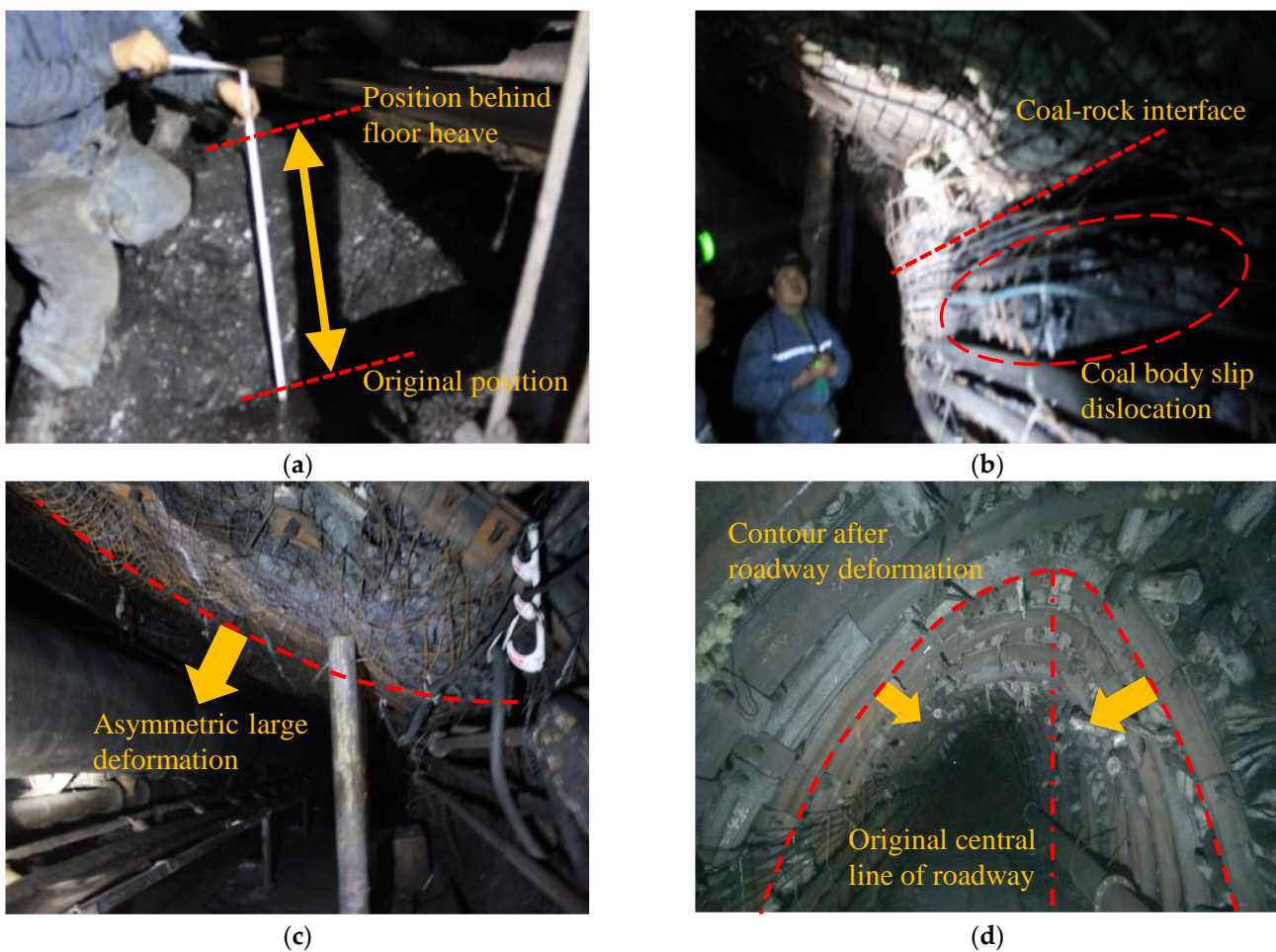**Figure 1.** Pictures of roadway deformation characteristics. (**a**) Continuous floor heave; (**b**) coal–rock interface slip dislocation; (**c**) asymmetrical failure of bolt–mesh–anchor support; (**d**) asymmetrical failure of U-shaped steel support.
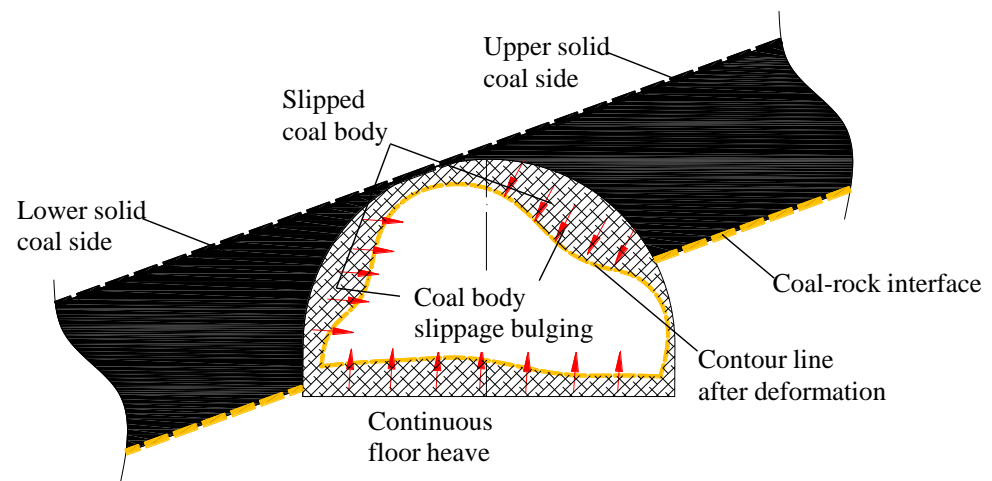
Figure 2. Sketch of asymmetric deformation characteristics of roadway.

3. Engineering Geology Overview

The 1511 return airflow roadway of a mine in Guizhou is arranged in the No. 15 coal seam and floor strata of the mine. The roadway protection method of gob-side entry driving with 3 m wide and narrow coal pillars has been adopted. The roof and floor are mainly mudstones, argillaceous siltstone and other weak strata. The layout and thickness of the rock strata are shown in Figure 3. The average thickness of the coal seam is 2.1 m, and the average dip angle is 20°. The cross-section shape of the roadway is a straight walled semicircular arch, and the net size of the cross-section is 5000 mm × 3100 mm (lower width × middle height). The coal part accounts for about 60% of the cross-section size area, it belongs to the typical GCRGICS. The main mechanical parameters of the coal seam and strata are shown in Table 1.

| Lithology	Column	No.	Thickness (m)	Lithological characters
Siltstone		1	10	Gray, medium-thick bedded, containing calcareous cements
Argillaceous siltstone		2	3.0	Gray, thinly-bedded, containing plant fossil
No. 15 coal seam		3	2.0–2.4	Black, mainly semidull coal, vitreous luster, brittleness, most blocky
Argillaceous siltstone		4	1–2	Gray, thinly-bedded, containing plentiful plant fossil
Fine sandstone		5	3–4	French grey, medium-thick bedded, brittleness

Figure 3. Lithological column of the gob-side coal–rock roadway.

Table 1. Mechanical parameters of coal seam and strata.

Lithology	Density (g/cm³)	Bulk (GPa)	Shear (GPa)	Cohesion (MPa)	Friction (°)
Overlying strata	2.500	12.00	7.60	2.30	28
Siltstone	2.325	10.85	7.00	7.90	31
Argillaceous siltstone	2.370	11.90	7.80	8.60	33
No. 15 coal seam	1.395	0.75	0.23	0.21	13
Fine sandstone	2.325	10.85	7.00	7.90	31
Underlying strata	2.500	12.00	7.60	2.30	28

4. Asymmetric Deformation Mechanism of Coal–Rock Interface Slip Dislocation under the Influence of Dip Angle

By summarizing the deformation and failure characteristics of the roadway, it can be seen that the deformation of the roadway was mainly located on the coal side, and the coal side deformation was mainly composed of the slip and dislocation of the coal–rock interface. Some scholars have studied mining stress and the mechanical properties of the coal pillar, the literature [25,26] established two different analytical models, respectively, to determine the mining stress of the roadways and the pillars, and mathematically, the transferred stress and coefficient of stress concentration over roadways and pillars were determined. The literature [27] proposed that the strength of an inclined coal pillar should be estimated by considering the dip angle of the coal seam and its related characteristics because the shear effect along the dip angle will aggravate the instability of the inclined coal pillar. In order to analyze the shear–slip dislocation mechanism of the coal–rock interface of the roadway side of the GCRGICS, a simplified model of the mechanics (Figure 4) was established by considering only the coal–rock interface between the narrow coal pillar and the floor, taking the narrow coal pillar side as the object of study. In the figure, σ_y is the normal y-direction stress at the coal–rock interface in the narrow coal pillar (Mpa); σ_x is the x-direction stress along the coal–rock interface in the narrow coal pillar (Mpa); α is the dip angle of the coal seam (°).
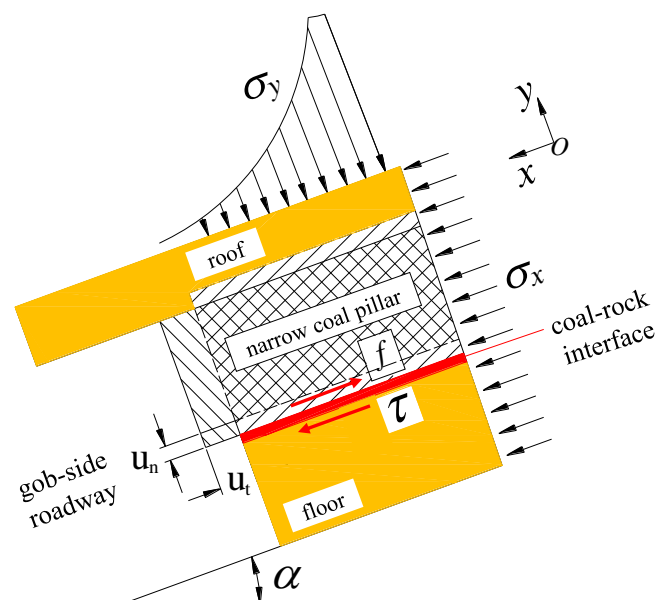
Figure 4. Mechanical model of shear–slip fault of coal–rock interface of the narrow coal pillar side.

The tendency of relative slip dislocation at the coal–rock interface will generate two types of forces. One is shear stress τ caused by σ_x stress along the coal–rock interface direction, the

other is friction stress f caused by normal stress σ_y along the coal–rock interface direction. The relationship between the two forces can be expressed by an empirical equation [28].

$$\tau = \sigma_y \tan\left[\text{JRClg}\left(\frac{\text{JCS}}{\sigma_y}\right) + \varphi_b\right] \tag{1}$$

where JRC and JCS are the roughness coefficient and compressive strength of the coal–rock interface, respectively, and φ_b is the basic internal friction angle of the rock.

Due to the influence of strength difference, the coal body above the coal–rock interface will first produce normal displacement u_y under normal stress σ_y and quickly reach the limit value. After that, the shear displacement u_x is continuously generated along the coal–rock interface under the shear stress τ. It can be expressed by the following equation [2,29,30].

$$u_y = u_{\max}\left[1 - \exp\left(-\frac{\sigma_y}{k_{n0}}\right)\right] \tag{2}$$

$$u_{\max} = H + I(\text{JRC}) + J\left(\frac{\text{JCS}}{a_j}\right)^K \tag{3}$$

$$k_{n0} = -7.15 + 1.75(\text{JRC}) + 0.02\left(\frac{\text{JCS}}{a_j}\right) \tag{4}$$

$$a_j = \frac{\text{JRC}}{5}\left(0.2\frac{\sigma_c}{\text{JCS}} - 0.1\right) \tag{5}$$

where $u_{\max}$ is the maximum normal closure quantity of coal–rock interface (m); k_{n0} is the initial normal stiffness of the coal–rock interface (N/m); H, I, J, K are regression coefficients; and σ_c is the uniaxial compressive strength (Mpa).

The following relationship between the normal stress σ_y at the coal–rock interface and the stress σ_x along the coal–rock interface in the x direction.

$$\sigma_x = \lambda\sigma_y \tag{6}$$

where λ is the lateral pressure coefficient along the x direction of the coal–rock interface.

During the service of the GCRGICS, σ_y and σ_x rise sharply due to excavation disturbance and surrounding rock stress concentration, which accelerates the increase of shear stress τ at the coal–rock interface. When τ and friction stress f satisfy Equation (7), the slip dislocation deformation of the coal body will occur along the coal–rock interface. The relationship between the shear displacement u_x and the shear stress τ can be expressed by the hyperbolic equation, Equation (8) [16].

$$\tau \geq f = \sigma_y \tan\left[\text{JRClg}\left(\frac{\text{JCS}}{\sigma_y}\right) + \varphi_b\right] \tag{7}$$

$$\tau = \frac{u_x}{m + nu_x} \tag{8}$$

where m and n are the reciprocal of the shear stiffness K_{si} and the reciprocal of the hyperbolic horizontal asymptotic line, respectively.

Therefore, after the roadway is dug out, the coal–rock interface of the two sides is mainly dominated by the shear–slip dislocation deformation of the coal body, which becomes the main channel for the release of stress and deformation energy. Affected by the shear stress τ of the coal–rock interface, the larger the shear stress is, the larger the amount of shear–slip deformation produced. Moreover, the shear stress is mainly caused by the stress σ_x along the direction of the coal–rock interface. In other words, under the same conditions, the larger σ_x is, the more obvious the tendency of shear–slip dislocation deformation.

Different from a near-horizontal coal seam, mining the gently inclined coal seam produces a self-weight stress component σ_{zx} along the coal–rock interface. Obviously, when σ_{zx} is the same or opposite direction of stress σ_x along the coal–rock interface direction, the effect of σ_x will be intensified or weakened, resulting in differences in the amount of shear–slip misalignment deformation induced in the coal–rock interface. Therefore, for the upper side of the GCRGICS, since the stress component of the self-weight stress of the narrow coal pillar along the coal–rock interface is the same as that of σ_x, it will aggravate the slip dislocation deformation of the coal body to the roadway space. For the lower solid coal side, the self-weight stress along the stress component of the coal–rock interface is opposite to the σ_x direction, which will slow down the deformation trend to a certain extent. Combined with the influence of the strength difference of the upper and lower sides of the gob-side roadway, the shear–slip dislocation deformation of the upper and lower sides of the coal–rock interface is expanded, which is the internal direct cause of asymmetric deformation and failure of the surrounding rock.

5. Numerical Simulation of Asymmetric Deformation and Failure Characteristics of the GCRGICS under Different Dip Angles

5.1. Establishment of Numerical Calculation Mode

The deformation and failure of the surrounding rock of the GCRGICS was a three-dimensional spatiotemporal evolution process, so the finite-difference software FLAC^{3D} was used to establish a three-dimensional numerical calculation model as shown in Figure 5, the model size (X × Y × Z) was 350 m × 120 m × 170 m. The coal seam and its immediate roof, main roof, immediate floor, main floor and other strata within 25 m around the roadway were used for local grid refinement, and the model was divided into 127,280 grids and 13,938 mesh nodes. The bottom of the model was fixed, the horizontal displacement was limited around the model and 7.5 MPa was applied on the top of the model to simulate the weight of the overlying strata on the buried depth of the roadway, and the Mohr–Coulomb yield criterion was selected for this structural model.
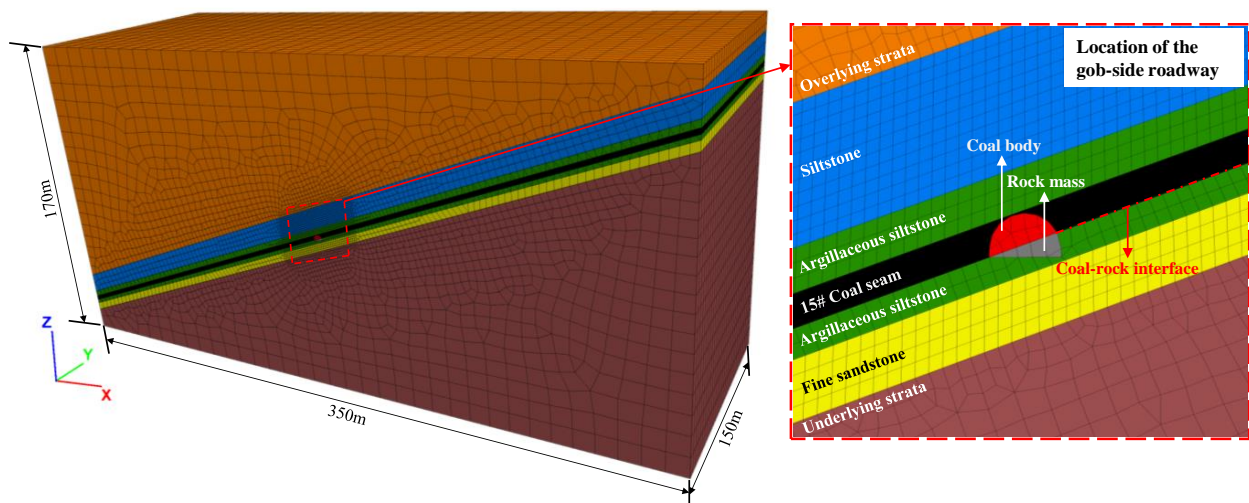

Figure 5. Three-dimensional numerical model.

In order to analyze the coal seam dip effect of asymmetric deformation and failure of the surrounding rock, four numerical models with dip angles of 0°, 10°, 20° and 25° were established, as shown in Figure 6.
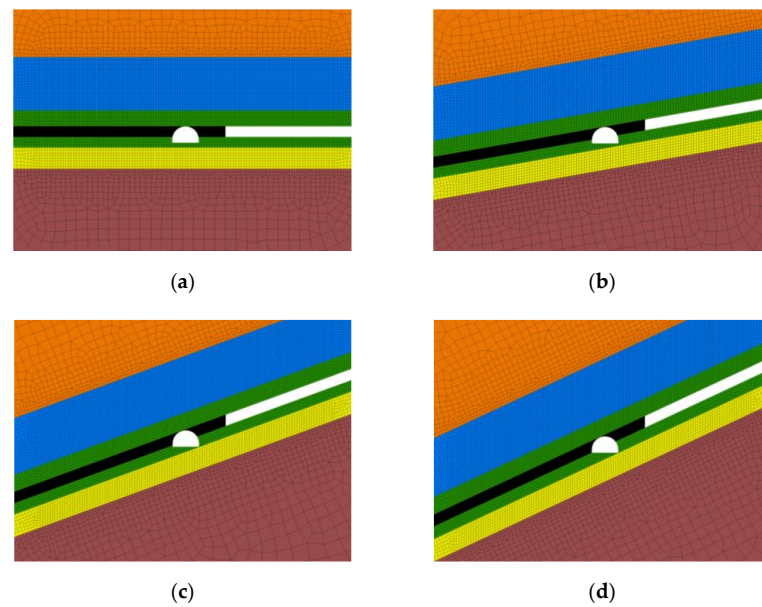
Figure 6. Numerical model with different dip angles of coal seam (partial). (**a**) $\alpha = 0°$; (**b**) $\alpha = 10°$; (**c**) $\alpha = 20°$; (**d**) $\alpha = 25°$.

5.2. Numerical Simulation Results

5.2.1. Asymmetric Deformation Characteristics of the Gob-Side Coal–Rock Roadway under Different Dip Angles

Figures 7–12 show the contour map of the vertical displacement of the surrounding rock, the deformation evolution law of the roof, floor and two sides of the coal–rock body and the evolution law of the asymmetric deformation rate after the disturbance was stable under different coal seam dip angles.
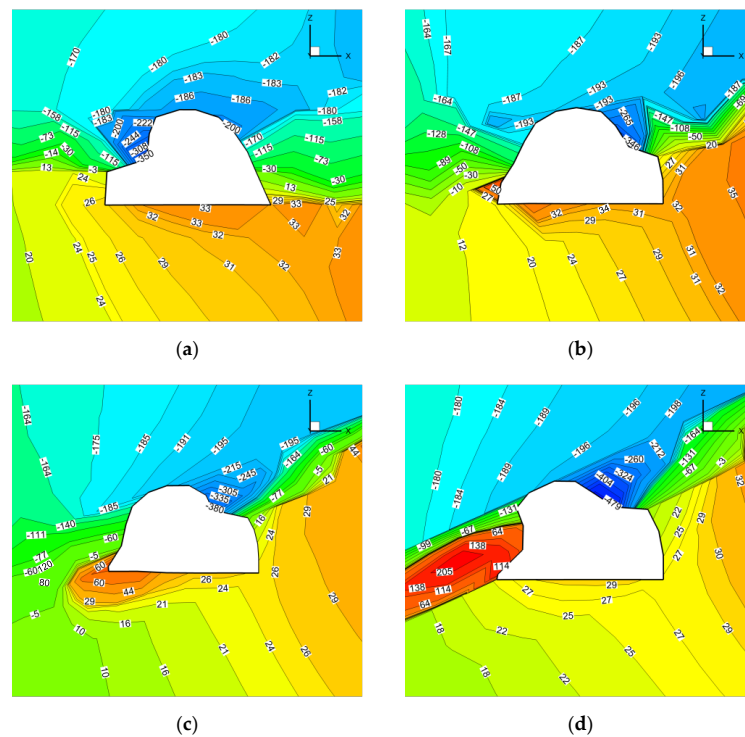

Figure 7. Vertical displacement contour map with different dip angles. (**a**) $\alpha = 0°$; (**b**) $\alpha = 10°$; (**c**) $\alpha = 20°$; (**d**) $\alpha = 25°$.
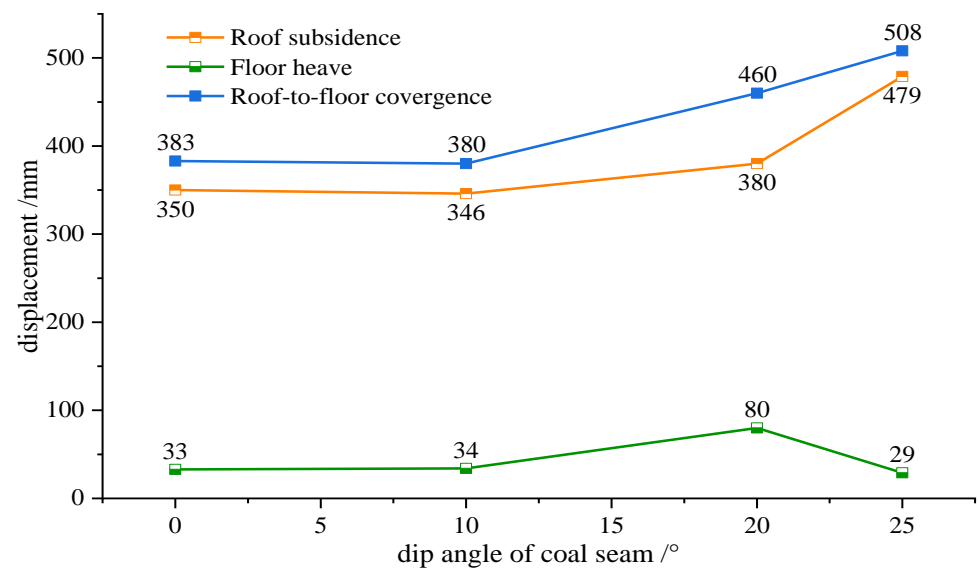
Figure 8. Deformation evolution law of surrounding rock with different dip angles of the coal seam (vertical displacement).

Figure 9. Horizontal displacement contour map with different dip angles. (**a**) $\alpha = 0°$; (**b**) $\alpha = 10°$; (**c**) $\alpha = 20°$; (**d**) $\alpha = 25°$.

Figure 10. Deformation evolution law of surrounding rock with different dip angles of the coal seam (horizontal displacement).
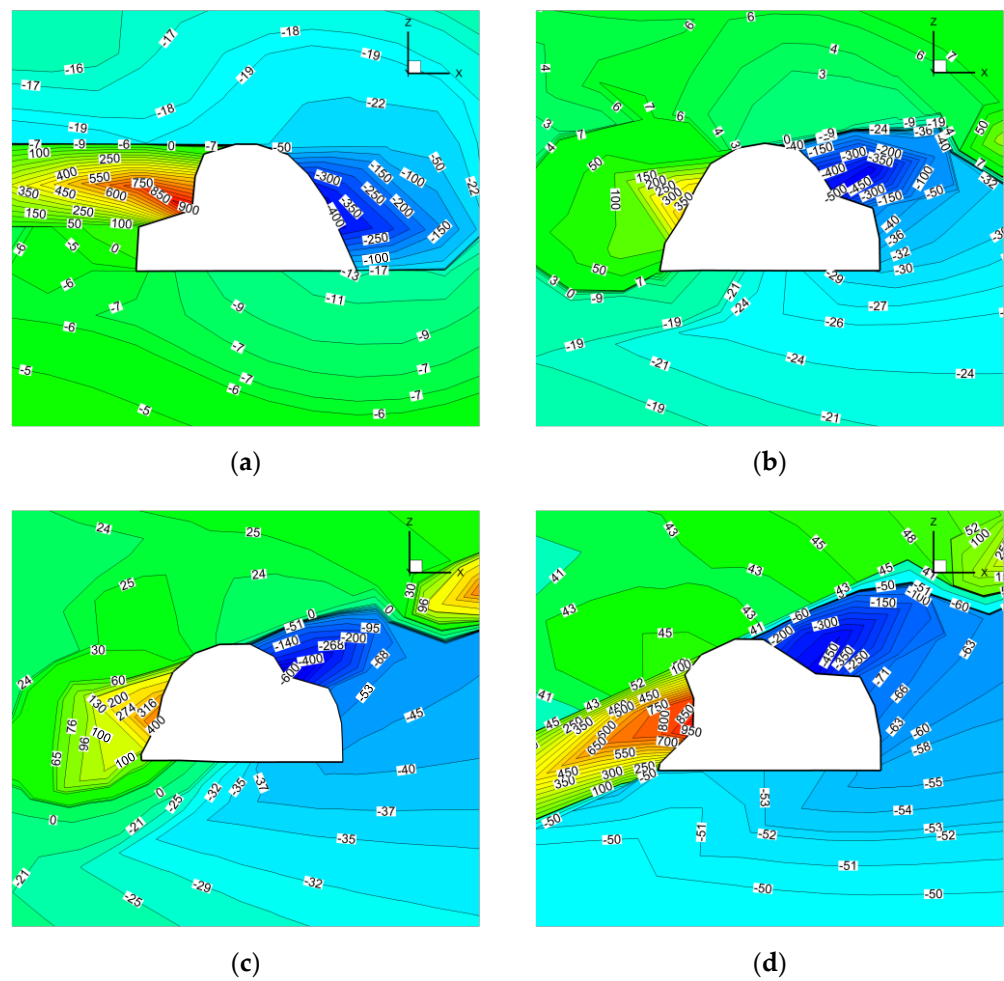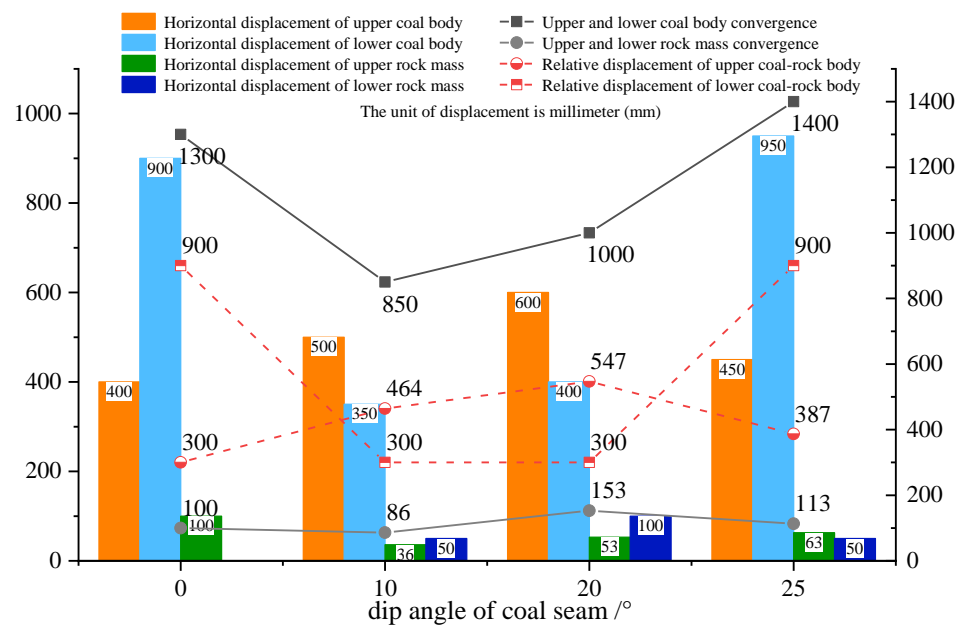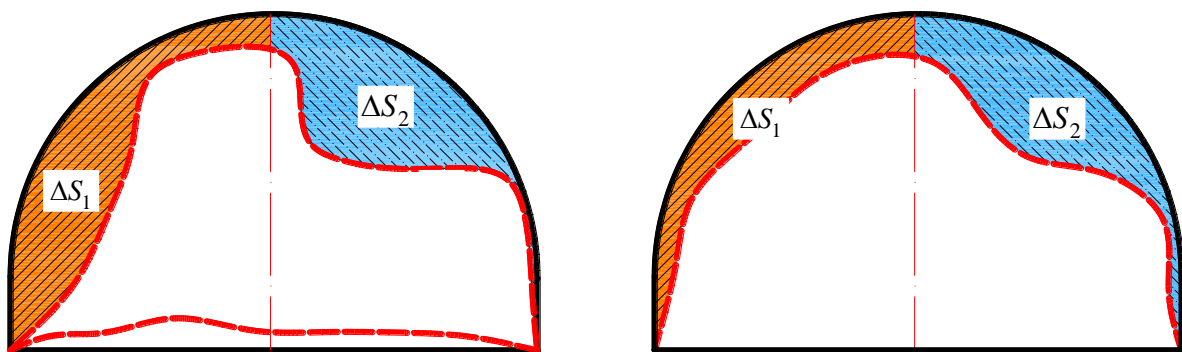

Figure 11. Conceptual model of asymmetric deformation rate.
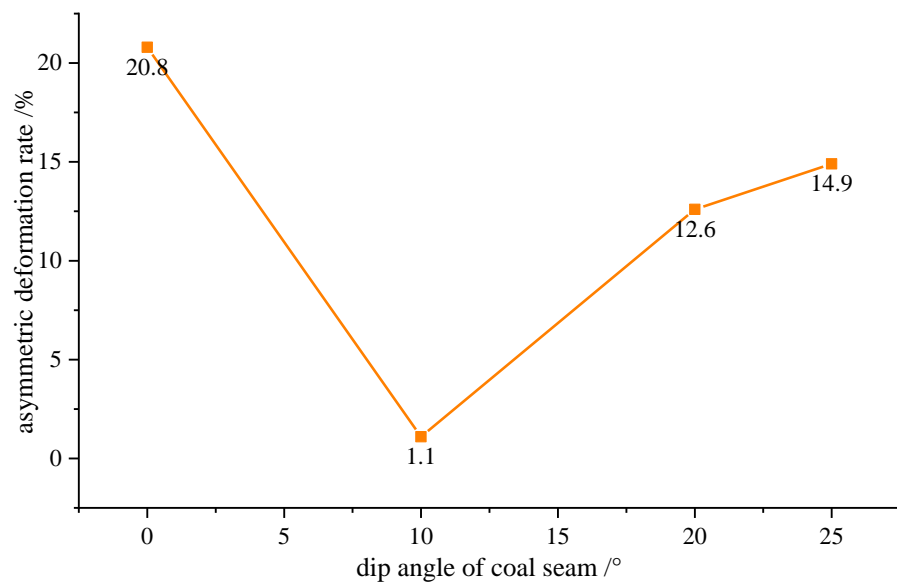

Figure 12. Evolution law of asymmetric deformation rate with different dip angles of the coal seam.

(1)   Vertical displacement

It can be seen from Figures 7 and 8 that, when the dip angle was 0°, the vertical deformation of the surrounding rock was dominated by the arc triangle coal on the solid coal side. The second was the arc triangle coal on the goaf side, and the maximum subsidence sizes were 350 and 200 mm, respectively. The deformations of the two sides of rock mass were small and the difference was small, and the deformation of floor heave was only 33 mm. At the coal–rock interface between the two sides of the roadway, the upper and lower sides of the coal and rock bodies showed discontinuous deformation. The vertical displacement of the upper coal body was downward, and the vertical displacement of the lower rock mass was upward, and the "vertical zero displacement" dividing line appeared in the area near the coal–rock interface.

As the dip angle gradually increased from 0° to 10°, 20° and 25°, the vertical displacement of the surrounding rock was still dominated by the roof subsidence but compared with the dip angle of 0°, the maximum subsidence of the roof turned to the arc triangle coal area on the upper side of the goaf, and the maximum subsidence sizes were 346, 380 and 479 mm. The second was the deformation of the lower rock mass, which were 50, 60 and 114 mm in turn. The deformations of the upper rock mass and floor heave were small and had little change; they remained at 20–30 and 30–40 mm, respectively. Moreover, with the increase of dip angle, the vertical displacement of the surrounding rock on both sides of the roadway still had obvious boundary characteristics near the coal–rock interface, and the boundary line of "vertical zero displacement" on both sides gradually rotated with the inclination direction of coal seam from the approximate horizontal position.

(2)   Horizontal displacement

It can be seen from Figures 9 and 10 that, when the dip angle was 0°, the horizontal deformation of the surrounding rock was dominated by the slip bulging deformation of the arc triangle coal on the solid coal side, and the maximum horizontal displacement reached 900 mm. The second was the arc triangle coal and rock mass on the goaf side, and the bulging amounts were 400 and 100 mm, respectively. The deformation of rock mass on the solid coal side was small, only 0–5 mm. The coal and rock bodies above and below the coal–rock interface of the two sides showed the deformation characteristics of sliding dislocation steps due to uncoordinated horizontal deformation, which was more obvious on the solid coal side.

As the dip angle gradually increased from 0° to 10° and 20°, the horizontal displacement of the surrounding rock began to transform into the slip bulging deformation of the arc triangle coal on the goaf side of the upper side, with the horizontal displacement reaching 500 and 600 mm, respectively. The second was the arc triangle coal on the lower solid coal side, with the horizontal bulging deformation reaching 350 and 400 mm, respectively. The deformation of the upper rock mass was small and had little change; it was 36 and 53 mm, respectively, and that of the lower rock mass was 50 and 151 mm, respectively. The overall surrounding rock presented an asymmetric large deformation trend characterized by the slip dislocation of the coal–rock interface, and the relative slip dislocation deformation of the upper coal–rock body was 464 and 547 mm, respectively.

When the dip angle increased to 25°, the coal and rock strata of the surrounding rock showed obvious inclination characteristics. Compared with the dip angle of 10° and 20°, the deformation of the surrounding rock changed significantly, again manifested as the deformation of the surrounding rock with the lower side arc triangle coal slip bulge; the maximum deformation was 950 mm. The second was the arc triangle coal on the upper side; the bulging deformation was 450 mm, and the deformation of the rock mass in the upper and lower sides was small, about 50–60 mm. The relative dislocation deformation of the upper and lower sides of the coal and rock bodies were 387 and 900 mm, respectively, and the asymmetric large deformation trend of the surrounding rock was further highlighted.

(3)   Asymmetric deformation rate

The complexity of underground mining conditions in coal mines presents more types of roadways with asymmetric deformation characteristics, but their analysis has been mostly described qualitatively in the past.

In order to further analyze the quantitative correlation between the asymmetric deformation characteristics and the influencing factors of the GCRGICS and to seek the quantitative control and evaluation method, the literature [31] proposed the concept of "asymmetric deformation rate" and quantitatively characterized the degree of asymmetric deformation by the relative difference in degree of deformation between the two sides of the roadway, calculated as shown in Equation (9).

$$\eta = \frac{\max(\Delta S_1, \Delta S_2) - \min(\Delta S_1, \Delta S_2)}{\min(\Delta S_1, \Delta S_2)} \times 100\% \tag{9}$$

where ΔS_1 and ΔS_2 are the shrinkage of the two sides of the roadway bounded by the center line of the original roadway section, (m^2). As shown in Figure 11, $\Delta S_1 = S_1 - S_1{}' \geq 0$, $\Delta S_2 = S_2 - S_2{}' \geq 0$. Among them S_1, S_2 and $S_1{}'$, $S_2{}'$ are the original design section area on both sides of the roadway bounded by the original roadway center line and the section area after contraction, respectively (m^2). Obviously, the larger η is, the more obvious the asymmetric deformation characteristics of the roadway.

(4)   Evolution law of asymmetric deformation rate

It can be seen from Figure 12 that, in the inclination angle range of 0°–25°, the asymmetric deformation rate of the gob-side coal–rock roadway and the inclination angle of the coal seam were roughly V-shaped. When the dip angle of the coal seam was 0°, the deformation of the surrounding rock was mainly the slip dislocation deformation of the coal body of the solid coal side, and the asymmetric deformation rate was larger, which was 20.8%.

When the dip angle increased to about 10°, the deformation difference on both sides of the roadway decreased due to the obvious increase of the slip dislocation deformation of the upper coal body, and the asymmetric deformation rate decreased significantly to 1.1%. When the coal seam dip angle further increased to 20° and 25°, the slip dislocation deformation of the lower side of the roadway increased significantly due to the increase in coal area, and the asymmetric deformation rate increased to about 15%. Therefore, for the GCRGICS, from the perspective of reducing the asymmetric deformation rate, it was more favorable when the coal seam dip was about 10°, while the asymmetric deformation characteristics were more obvious when the coal seam dip was too small or too large.

5.2.2. Asymmetric Failure Characteristics of the Gob-Side Coal–Rock Roadway under Different Dip Angles

The distribution of the plastic zone of the surrounding rock after the influence of driving and mining disturbance stabilization at different dip angles is shown in Figure 13.

When the dip angle was 0°, the plastic zone range of the surrounding rock on the solid coal side was larger than that on the goaf side and was dominated by shear failure. The plastic zone of the floor was symmetrically distributed and mainly underwent shear failure. The surrounding rock of the two sides was affected by the strength difference between the coal and rock bodies, the arc triangle coal area was characterized by tensile–shear composite failure. The shear failure was the main part of the roadway, and the deformation and failure of the roadway were mainly concentrated in the solid coal side area.

With the dip angle increased to 25°, compared with 0°, the plastic zone range of the roadway roof and its two sides expanded continuously, and it showed that the failure range of the surrounding rock of the gob-side roadway increased significantly with the increase of the coal seam dip angle. The plastic zone of the floor was mainly concentrated in the floor area near the solid coal side, and with the increase of dip angle, it gradually shifted

from the symmetric distribution to the asymmetric distribution, and the trend was more obvious, indicating that the dip angle was closely related to the failure mode of the floor.
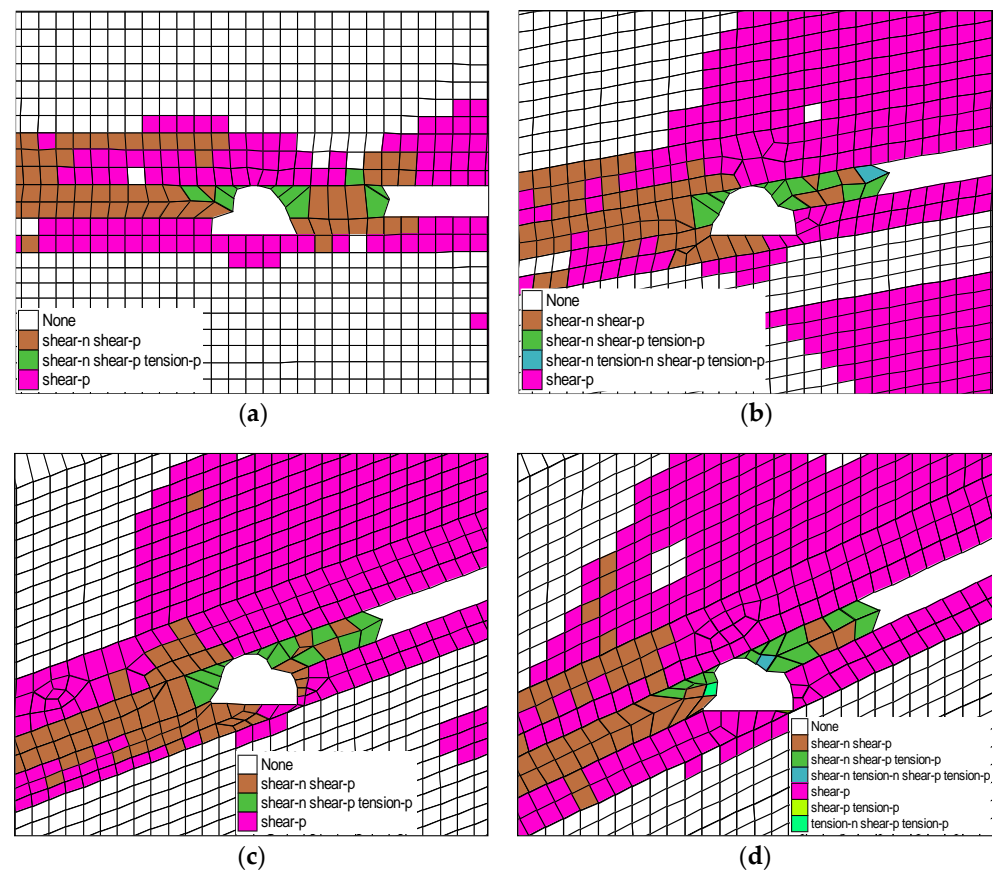

Figure 13. Plastic zone distribution with different dip angles. (**a**) $\alpha = 0°$; (**b**) $\alpha = 10°$; (**c**) $\alpha = 20°$; (**d**) $\alpha = 25°$.

6. Conclusions

(1) This study found the influence law of the dip angles on the asymmetric deformation and failure of the surrounding rock of the gob-side coal–rock roadway. With the increase of the dip angle, the shear–slip dislocation deformation of the coal–rock interface intensified. The deformation of the upper coal body slippage and misalignment was increased, the narrow coal pillar yielded instability gradually, and the surrounding rock stress transferred to the lower solid coal side. The maximum slip deformation area gradually transferred from the upper arc triangle coal to the lower arc triangle coal, and the asymmetric deformation characteristics of the surrounding rock were more obvious.

(2) For the GCRGICS, the relationship between asymmetric deformation rate and coal seam dip angle was roughly V-shaped. When the coal seam dip angle was 10°, the asymmetric deformation rate was the smallest, only 1.1%. When the coal seam dip angles were 0°, 20° and 25°, due to the difference of slip dislocation deformation between the solid coal side and the upper goaf side, the asymmetric deformation rates were relatively large, 20.8%, 12.6% and 14.9%, respectively.

(3) The plastic zone range of the surrounding rock expanded with the increase of the dip angle, it showed that the failure range of the surrounding rock of the gob-side roadway increased significantly after the increase of the dip angle. The new expansion range was mainly located in the roof area, and the plastic zone of the floor was mainly concentrated on the side of solid coal and developed from symmetric distribution to asymmetric distribution with the increase of dip angle.

(4) Compared with the existing research on the coal–rock roadways, the significance of this study was to provide a scientific basis and theoretical guidance for the formulation of the surrounding rock control scheme of the gob-side coal–rock roadway under different dip angles. For the asymmetric deformation roadways under different dip angles, the asymmetric support designs should be carried out according to the load distribution law of the surrounding rock, such as anchor cable reinforcement support or adjustment of bolt (cable) support parameters for differential support countermeasures, so as to realize the strength coupling between the support body and the surrounding rock and make the surrounding rock and the support body uniformly and harmoniously deform within the allowable range of engineering application.

Institutional Review Board Statement: The study did not require ethical approval.

Informed Consent Statement: Informed consent was obtained from all subjects involved in the study.

Data Availability Statement: All data and/or models used in the study appear in the submitted article.

Conflicts of Interest: The authors declare no conflict of interest.

References

1. Gao, L.; Wang, J.C.; Kong, D.Z.; Wu, G.Y.; Ma, Z.Q. Deformation mechanism and repairing technology for coal-rock uphill roadway under influence of dynamic pressure. *China Saf. Sci. J.* **2020**, *30*, 67–73.
2. Yu, W.J.; Feng, T.; Wang, W.J.; Wang, P.; Yuan, C.; Guo, G.Y.; Du, S.H. Support problems and solutions of roadway surrounding rock for thin coal seams under complex conditions in Southern China. *J. China Coal Soc.* **2015**, *40*, 2370–2379.
3. Gao, L.; Zhao, S.H.; Huang, X.F.; Ma, Z.Q.; Kong, D.Z.; Kang, X.T.; Han, S. Experimental study on surrounding rock characteristics of gateway in Panjiang mining area. *J. GZU (Nat. Sci.)* **2022**. Available online: http://kns.cnki.net/kcms/detail/52.5002.N.2022 0412.0956.002.html (accessed on 13 April 2022).
4. Zhang, P.D.; Gao, L.; Liu, P.Z.; Wang, Y.Y.; Liu, P.; Kang, X.T. Study on the influence of borehole water content on bolt anchoring force in soft surrounding rock. *Shock Vib.* **2022**, *2022*, 2384626. [CrossRef]
5. Yu, W.J.; Feng, T.; Wang, W.J.; Liu, H.; Ma, P.Y.; Wang, P.; Li, R.H. Deformation mechanism, control principle and technology of soft half coal rock roadway. *Chin. J. Rock Mech. Eng.* **2014**, *33*, 658–671.
6. Majdi, A.; Rezaei, M. Prediction of unconfined compressive strength of rock surrounding a roadway using artificial neural network. *Neural Comput. Appl.* **2013**, *23*, 381–389. [CrossRef]
7. Jin, G.; Wang, L.G.; Li, Z.L.; Zhang, J.H. Study on the gateway rock failure mechanism and supporting practice of half-coal-rock extraction roadway in deep coal mine. *J. Min. Saf. Eng.* **2015**, *32*, 963–967.
8. Wang, M.; Xiao, T.Q.; Gao, J.; Liu, J.L. Deformation mechanism and control technology for semi coal and rock roadway with structural plane under shearing force. *J. Min. Saf. Eng.* **2017**, *34*, 527–534.
9. Liu, C.X. Research of imitating the numerical calculation on rock structure stability of half coal seam roadway. *J. Basic Sci. Eng.* **2000**, *8*, 16–21.
10. Yao, Q.; Feng, T.; Wang, W.J.; Yu, W.J.; Wang, P.; Yuan, C. Study on deformation and failure mechanism and support control measure of half coal rock roadway under extremely fractured surrounding rock. *J. Saf. Sci. Technol.* **2015**, *11*, 32–39.
11. Zhang, H.L.; Wang, L.G.; Tu, M. Failure evolution laws and control technology of roadway surrounding rock. *J. Heilongjiang Inst. Sci. Technol.* **2013**, *23*, 258–262.
12. Jin, G.; Hao, G.S. Numerical simulation of anchored rope supporting in half-coal and half-rock roadway. *Coal Min. Technol.* **2012**, *17*, 55–58.

13. Luo, J.A.; Wang, L.G.; Hou, H.Q. Preliminary research on coal-rock structural plane of mining roadway located in thin coal seam. *Min. Res. Dev.* **2014**, *34*, 22–26.
14. Wang, H.; Jiang, C.; Zheng, P.Q.; Zhao, W.J.; Li, N. A combined supporting system based on filled-wall method for semi coal-rock roadways with large deformations. *Tunn. Undergr. Space Technol.* **2020**, *99*, 103382. [CrossRef]
15. Sun, Y.N.; Zhou, H.C.; Zhou, J.R.; Xiong, Z.Q. Control technique of floor heave in semi coal and rock roadway with weak floor. *J. Min. Saf. Eng.* **2007**, *24*, 340–344.
16. Yu, W.J.; Wu, G.S.; Liu, H.; Wang, P.; An, B.F.; Liu, Z.; Huang, Z.; Liu, F.F. Deformation characteristics and stability control of soft coal-rock mining roadway in thin coal seam. *J. China Coal Soc.* **2018**, *43*, 2668–2678.
17. Xu, T.B. Surrounding rock control technique in semi-coal and semi-rock roadway with ultra long distance. *J. Min. Saf. Eng.* **2009**, *26*, 168–172.
18. Gao, L.; Liu, P.Z.; Zhang, P.D.; Wu, G.Y.; Kang, X.T. Influence of fracture types of main ro-of on the stability of surrounding rock of the gob-side coal-rock roadway in inclined coal seams and its engineering application. *Goal Geol. Explor.* **2022**. Available online: https://kns.cnki.net/kcms/detail/61.1155.p.20220416.0838.002.html (accessed on 20 April 2022).
19. Zhang, N.; Li, B.Y.; Li, G.C.; Qian, D.Y.; Yu, X.Y. Inhomogeneous damage and sealing support of roadways through thin bedded coal-rock crossovers. *J. Min. Saf. Eng.* **2013**, *30*, 1–6.
20. Yang, X.P.; Xie, X.P.; Liu, X.N. Comprehensive control technology of floor heave in soft floor roadway of semi coal rock. *Saf. Coal Mines* **2013**, *44*, 78–81.
21. He, X.K.; Wei, S.J.; Gao, J.H. Numerical simulation optimization on parameters of bolt support in semi coal and rock roadways. *J. HPU (Nat. Sci.)* **2009**, *28*, 705–708.
22. Li, J.F.; Guo, W.Y.; Zhang, C.L.; Cheng, C.X.; Liu, J.K.; Zhou, G.L. Supporting Technology of fully mechanized half-coal rock mining roadway in thin seam. *Saf. Coal Mines* **2013**, *44*, 97–99, 103.
23. Zheng, Y.; He, C.C.; Xi, C.D.; Yao, B.; Liu, B.H. Analysis on numerical simulation of anchor setting parameters in the semi-coal and semi-rock roadway. *Coal Chem. Ind.* **2015**, *38*, 90–92.
24. Cui, Q.L.; Wu, J.X. Parameters optimization of bolting in mining coal-rock roadway under shallow overburden. *Coal Eng.* **2015**, *47*, 48–50.
25. Rezaei, M.; Hossaini, M.F.; Majdi, A. Determination of longwall mining-induced stress using the strain energy method. *Rock Mech. Rock Eng.* **2015**, *48*, 2421–2433. [CrossRef]
26. Rezaei, M.; Hossaini, M.F.; Majdi, A. Development of a time-dependent energy model to calculate the mining-induced stress over gates and pillars. *J. Rock Mech. Geotech. Eng.* **2015**, *12*, 306–317. [CrossRef]
27. Das, A.J.; Mandal, P.K.; Paul, P.S.; Sinha, R.K. Generalised analytical models for the strength of the inclined as well as the flat coal pillars using rock mass failure criterion. *Rock Mech. Rock Eng.* **2019**, *52*, 3921–3946. [CrossRef]
28. Barton, N. Review of a new shear-strength criterion for rock joints. *Eng. Geol.* **1973**, *7*, 287–332. [CrossRef]
29. Bandis, S.C.; Lumsden, A.C.; Barton, N.R. Fundamentals of rock joint deformation. *Int. J. Rock Mech. Min. Sci.* **1983**, *20*, 249–268. [CrossRef]
30. Rezaei, M.; Hossaini, M.F.; Majdi, A. A time-independent energy model to determine the height of destressed zone above the mined panel in longwall coal mining. *Tunn. Undergr. Space Technol.* **2015**, *47*, 81–92. [CrossRef]
31. Gao, L. Asymmetric Deformation Characteristics and Failure Mechanism of the Gob-Side Coal-Rock Roadway and Its Control Techniques in Gently Inclined Coal Seam. Ph.D. Thesis, China University of Mining and Technology, Beijing, China, 2020.